Patient Dosimetry of Intravenously Administered ^{99m}Tc-Annexin V

Gerrit J. Kemerink, Ing Han Liem, Leo Hofstra, Hendrikus H. Boersma, Wil C.A.M. Buijs, Chris P.M. Reutelingsperger, and Guido A.K. Heidendal

Departments of Nuclear Medicine, Cardiology, and Clinical Pharmacology and Toxicology, University Hospital Maastricht, Maastricht; Department of Nuclear Medicine, University Medical Center Nijmegen, Nijmegen; and Department of Biochemistry, Cardiovascular Research Institute, University of Maastricht, Maastricht, The Netherlands

Annexin V labeled with ^{99m}Tc is evaluated as a potential in vivo marker for tissue with increased apoptosis. Promising results in patients have been obtained with ^{99m}Tc-(n-1-imino-4-mercaptobutyl)-annexin V (^{99m}Tc-i-AnxV). Because information on biodistribution and radiation burden is desired for the application of any radiopharmaceutical, a dosimetric study of ^{99m}Tc-i-AnxV was undertaken. **Methods:** Eight persons with normal kidney and liver functions were included in this study: six patients with myocardial infarction, one with Crohn's disease, and one healthy volunteer. Approximately 600 MBq ^{99m}Tc-i-AnxV were injected intravenously immediately before a dynamic study with a dual-head gamma camera in conjugate view mode. In the next 24 h, two to four whole-body scans were acquired. Patient thickness was determined from a transmission scan with a ^{57}Co flood source. Organ uptake was estimated after correction for background, attenuation, and scatter, using a depth-independent buildup factor and an organ-size–dependent attenuation correction. Residence times were calculated from the dynamic and whole-body studies and used as input for the MIRDOSE 3.1 program to obtain organ-absorbed doses and effective dose. **Results:** Activity strongly accumulated in the kidneys (21% ± 6% of the injected dose at 4 h postinjection) and the liver (12.8% ± 2.2%). Uptake in the target tissues (myocardium or colon) was limited and negligible from a dosimetric point of view. The biologic half-life of activity registered over the total body was 62 ± 13 h. Of the excreted activity, ~75% went to the urine and 25% to the feces. The absorbed dose for the more strongly exposed organs was (in μGy/MBq): kidneys, 93 ± 24; spleen, 22 ± 6; liver, 17 ± 2; testes, 15 ± 3; thyroid, 10 ± 6; urinary bladder wall, 7.5 ± 2.6; and red bone marrow, 5.5 ± 0.8. The effective dose was 9.7 ± 1.0 μSv/MBq, corresponding to a total effective dose of 5.8 ± 0.6 mSv for a nominally injected activity of 600 MBq. **Conclusion:** ^{99m}Tc-i-AnxV strongly accumulates in the kidneys and to a lesser degree in the liver. The associated effective dose per MBq is in the midrange of values found for routine ^{99m}Tc-labeled compounds. From a dosimetric point of view ^{99m}Tc-i-AnxV is therefore well suited for the study of apoptosis in patients.

Key Words: radiation dosimetry; apoptosis; annexin V

J Nucl Med 2001; 42:382–387

Apoptosis is a genetically controlled process of cell suicide, which, on one hand, serves the homeostasis of the human organism, but, on the other hand, appears also to be involved in several pathologies, including the loss of heart muscle after cardiac ischemia and reperfusion, autoimmune and neurodegenerative diseases, tumor growth, and antitumor therapies (*1*).

Fadok et al. (*2*) showed that, early during apoptosis, cells expose phosphatidylserine (PS) at their surfaces. This is in contrast to living cells, which stringently keep PS localized in the membrane leaflets that face the cytosol (*3*). Annexin V is a protein that binds selectively to PS (*4*). As a result of this property, annexin V binds to apoptotic cells in vitro (*5*) and in vivo (*6*). In vitro (*7*) as well as in vivo studies (*8*) have indicated that PS exposure during apoptosis is independent of the cell type and the apoptosis-inducing trigger.

Our understanding of the role of apoptosis in human pathogenesis and treatment of pathologies arises mostly from the investigation of biopsied materials. To gain a better understanding, we need alternative strategies that allow the measurement of apoptosis in situ by noninvasive techniques. One such technique is radionuclide imaging. Blankenberg et al. (*9,10*) showed the feasibility of using ^{99m}Tc-hydrazinonicotinamide (HYNIC)-annexin V for noninvasive measurement of apoptosis in several animal models. Recently our group successfully applied ^{99m}Tc-(n-1-imino-4-mercaptobutyl)-annexin V (^{99m}Tc-i-AnxV) to monitor scintigraphically cell death in the hearts of patients who received reperfusion therapy for acute myocardial infarction (*11*).

The applicability of the annexin V-PS concept to measure apoptosis in humans scintigraphically depends, among other things, on the biodistribution of the radiopharmaceutical and the associated radiation burden to the patient. It was therefore decided to complement our study of potential clinical applications of ^{99m}Tc-i-AnxV with an assessment of patient radiation dose. The results of this latter analysis, including some biodistribution data, are presented.

Received May 17, 2000; revision accepted Sep. 14, 2000.

For correspondence or reprints contact: Gerrit J. Kemerink, PhD, Department of Nuclear Medicine, University Hospital Maastricht, PO Box 5800, 6202 AZ Maastrich A, The Netherlands.

MATERIALS AND METHODS

This dosimetric study involved eight persons (six male, two female). The average age was 53 y (range, 34–66 y). Of the eight patients, six had myocardial infarction, one had Crohn's disease, and one was a healthy volunteer. Selection criteria included normal liver and kidney functions. The study was approved by the local medical ethics committee, and all patients gave informed consent.

The radiopharmaceutical was prepared by adding ~1,000 MBq ^{99m}Tc-pertechnetate to 1 mg freeze-dried (n-1-imino-4-mercaptobutyl)-annexin V (Mallinckrodt, Petten, The Netherlands). This mixture was incubated for 2 h at room temperature. Radiochemical purity was assessed by column chromatography using a Sephadex PD10-column (Pharmacia, Upsalla, Sweden) and 1% bovine albumin (Sigma, St. Louis, MO) in saline as eluant.

All patients were imaged with a dual-head gamma camera (Multispect 2; Siemens Gammasonics, Hoffman Estates, IL), equipped with high-resolution collimators. A 15% energy window around the photopeak of ^{99m}Tc was used. At the moment of intravenous injection of ^{99m}Tc-i-AnxV, a dynamic study was started, comprising 30–60 frames of 1 min each. The lower thorax–upper abdomen of the patient was imaged in conjugate anterior and posterior views. Subsequently, two to four whole-body scans were obtained, with a scan speed of 10 cm/min. The duration of the dynamic study and the number of whole-body scans depended on patient condition and the moment during the day the patient was presented at the department. Patients were not allowed to void before the first whole-body scan. The last whole-body study was acquired after 20–24 h. A ^{99m}Tc source of known activity was scanned together with the patient to monitor constancy of system sensitivity.

Blood samples were taken during the first 4 h to monitor the concentration of ^{99m}Tc in the circulatory system. The data were analyzed with a multicompartment model using least-squares weighted nonlinear regression analysis (MW/Pharm 3.30; Mediware, Groningen, The Netherlands). Urine was collected during the first hours while the patient was in the department. No feces were collected.

A transmission scan of all patients was performed with a ^{57}Co flood source at a time when the residual ^{99m}Tc activity in the patient had become fully negligible, or, as was the case in two studies, transmission was measured before injection of ^{99m}Tc-i-AnxV. The measured transmission was used to estimate patient thickness, using an attenuation coefficient of 0.125 cm^{-1}, a value found from transmission measurements on water phantoms of various thicknesses.

Regions of interest were drawn around all organs that showed noticeable uptake of ^{99m}Tc, around the bladder, and around the calibration source. A background region was defined for each organ. These same regions were duplicated in all other images, either by copying or mirroring as required. Subsequently, images and individual regions could be moved to achieve a proper fit of all regions around the corresponding organs in all images.

Background correction was performed as described by Buijs et al. (*12*). In this method background counts are corrected for finite organ thickness before subtraction from the organ counts. The organ thickness was approximated by the ratio of organ volume and the organ projection area as defined by the region that had been drawn. In this calculation, organ volume was taken as in the MIRD methodology (*13*). Patient thickness was derived from the average transmission within the organ region in the ^{57}Co scan. A correction was applied when patient thickness differed between organ and background position.

Absolute ^{99m}Tc organ activity was estimated by correcting measured counts for attenuation and scatter according to a method introduced by Siegel et al. (*14*). This method uses a depth-independent buildup factor in combination with an attenuation factor that is dependent on organ size. (For a review of methods in quantitative radiopharmaceutical biodistribution measurements, see reference *15*). System sensitivity was determined from a measurement of a petri disk with a known amount of activity, using the same camera settings and scan protocol as in the patient studies. Total body uptake was calculated using the "no patient excretion" approach. This means that the first whole-body scan was performed before the patient was allowed to void any activity. Division of the injected dose by the decay-corrected counts of the first total body scan yielded a "counts-to-fraction-of-injected-dose conversion factor." Multiplication of subsequently obtained total body counts with this factor gave an estimate of the total activity remaining in the body, expressed as a fraction of the injected dose. Organ uptake was calculated as the activity in the organ, corrected for physical decay, and was presented as a percentage of the injected dose (%ID).

To quantify excretion, all whole-body studies were inspected for activity in the colon. From the progress of activity in the colon, it was judged unlikely that relevant amounts of activity had been excreted in the feces within the first day. Consequently, activity that had left the body within the first 20 h must have been voided in the urine. Calling the fraction of the injected dose present in the colon at 20 h after injection $F_{colon,20h}$, and the fraction that had left the body $F_{urine,20h}$, the ratio $F_{colon,20h}/(F_{colon,20h} + F_{urine,20h})$ was taken as the fraction of the activity to be excreted through the intestinal trajectory.

Organ residence time was obtained by integrating the organ activity curve that was normalized with the injected dose but without correction for physical decay. In this calculation, subsequently measured points were used pairwise, that is, points 1 and 2, 2 and 3, etc., to derive analytic expressions for curve segments connecting these points, whereby the first function was extrapolated to time zero and the last to infinity. The fitted function was an exponential, because it was expected that the data, at least locally, could be approximated with this expression. This locally defined exponential was integrated analytically over the corresponding time interval, and the residence time was obtained by summation over all intervals.

For organs that were visible in the dynamic study, that is, the kidneys, liver, and spleen, the contribution to the residence time in the time interval corresponding to this study (i.e., from time zero to 30–60 min after injection) was substituted for the extrapolated residence time for this interval, which was derived from the whole-body studies. This is probably somewhat more accurate in case of a delayed wash-in or a fast washout. Bladder activity was excluded because, in the absorbed dose calculations, the dynamic bladder model was used (*16*). The residence time of the total body was calculated by integrating the normalized total-body activity, corrected for activity in the bladder and the activity of the calibration source. The residence time of the remainder of the body was then obtained by subtracting the residence time of all explicitly considered source organs except the bladder.

The dose to red bone marrow (RM) was calculated according to a method described by Buijs et al. (*17*), who defined regions around the iliac crests that were estimated to contain 25% of the

RM present in the pelvic bones, which contain ~17.5% of the total RM (*18*). The residence time of the activity in the iliac crests was thus multiplied with a factor of $(0.25 \times 0.175)^{-1} = 23$ to get the RM residence time. The residence time for blood was derived from a curve over the heart that had been normalized using blood samples taken in the first half-hour.

In the analysis, the region around the liver was drawn with exclusion of the part overlapping the right kidney. The right-kidney region covered the whole kidney, including the overlapping part of the liver. To correct at least partially for the errors made in this way, the residence time of the left kidney was subtracted from that of the right, and a positive difference, if any, was added to the residence time of the liver. This approach assumed that the uptake in the right kidney equals that in the left kidney, unless it is evident that this was not the case. In line with this, the residence time of the kidneys was taken as twice that of the left kidney, unless the sum of both kidneys was less.

To get an impression of the sensitivity of the estimated organ uptake to uncertainties in background correction and attenuation/scatter correction, the analysis was varied in a few ways. First, the effect of not applying background correction was investigated. Second, instead of Siegel's approach (*14*), we also estimated organ uptake using the "counts-to-fraction-of-injected-dose conversion factor" derived for the calculation of whole-body uptake. Third, in the calculation of the residence time, the interpolating function was also varied between exponential and linear. The latter approach is equivalent to integration using the trapezoidal rule.

The quantifications described above were performed with our own software developed on the Icon computer platform (Siemens Gammasonics). User interaction was largely limited to region definition and proper positioning of copies of these regions in all images.

Organ doses and effective dose were calculated using the MIRDOSE 3.1 program (*13*), applying the dynamic bladder model (*16*) with a voiding interval of 4 h and the individually measured biologic half-life.

RESULTS

The mean injected dose of ^{99m}Tc-i-AnxV was 551 ± 90 MBq, and the percentage of ^{99m}Tc bound to annexin V was 82% ± 12%.

In the infarcted area in the heart there was uptake of activity ($n = 6$), but in the case of Crohn's disease, no localized uptake could be discerned ($n = 1$). From a dosimetric point of view, however, the uptake of ^{99m}Tc-i-AnxV in the heart was negligible. Because, in addition, only patients with normal kidney and liver function were selected and no obvious differences in activity distribution were discernible, data from all persons were taken together in the dosimetric analysis.

Figure 1 shows, as an example, anterior and posterior views of the whole-body scan of the volunteer. Images showing uptake in regions with increased apoptosis have been published previously (*11*). In three patients, the number of whole-body scans was four; in another three patients, the number was three; and in two patients there were only two scans. The last two patients were presented at the end of the day.

FIGURE 1. Anterior (A) and posterior (B) views from whole-body scan of volunteer at 5 h after intravenous injection of 440 MBq ^{99m}Tc-i-AnxV.

In Figure 2 the average uptake, including the SD, is shown as a function of time for some source organs, including the left kidney, liver, and spleen. The blood curve shown is derived from total ^{99m}Tc activity in the blood samples. Because the whole-body scans differed in acquisition time and frequency, the measured data were interpolated on a fine-time grid. The interpolated curves were used in the calculation of the average and the SD.

The following are some pharmacokinetic parameters of decay-corrected ^{99m}Tc in blood ($n = 8$) during the first 4 h (these kinetics of the activity could be described using a two-compartment model with a fast and a slow component): for component α (fast), $t_{½}$ (minutes ± SD) = 14 ± 6, and fraction of the injected dose (±SD) = 0.52 ± 0.13; for component β (slow), $t_{½}$ (hours ± SD) = 4.1 ± 1.2 and fraction of the injected dose = 0.48 ± 0.13.

Table 1 presents the average uptake for all source organs at 4 h after intravenous injection. It is noted that

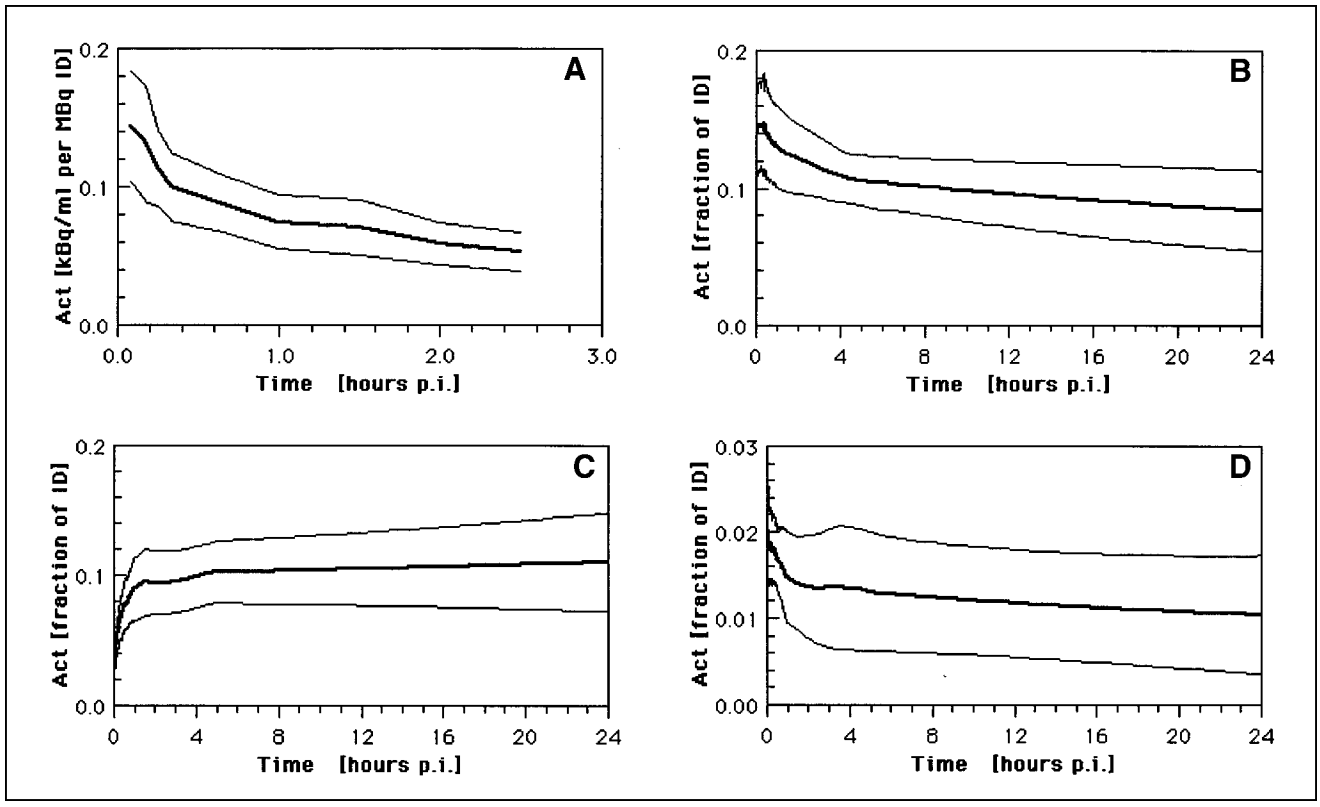

FIGURE 2. Decay-corrected time–^{99m}Tc uptake curves for blood (A), liver (B), left kidney (C), and spleen (D) after intravenous injection of ^{99m}Tc-i-AnxV. Curves with mean and mean ± 1 SD are shown.

the uptake within the right kidney region, which included some liver activity, was 11.5% ± 2.5%. Effective half-lives have also been calculated in Table 1. From these figures it is evident that the biologic half-life is long compared with the 6.02-h physical half-life of ^{99m}Tc (the biologic half-life may be obtained from $T_{biol} = [T_{effective} \times T_{phys}]/[T_{phys} - T_{effective}]$). In all organs uptake gradually diminishes over time, except in the kidneys and intestines, where uptake increases, at least during the first day. The residence time, the integral over time of the

TABLE 1
Dosimetric Data for Intravenously Administered ^{99m}Tc-i-AnxV
(n = 8)

Organ	Uptake at 4 h after injection* (%ID)	Effective half-life† (h)	Residence time (h)	Absorbed dose (μGy/MBq)
Kidneys	21.0 ± 5.6‡	6.3 ± 0.4	1.75 ± 0.40	93 ± 24
Liver	12.8 ± 2.2	5.5 ± 0.2	1.11 ± 0.15	17 ± 2
RM	4.2 ± 1.6	5.1 ± 0.4	0.34 ± 0.11	5.5 ± 0.8
Spleen	2.5 ± 1.3	5.2 ± 0.7	0.17 ± 0.08	22 ± 6
Testes (n = 6)	0.51 ± 0.10	5.1 ± 0.5	0.042 ± 0.009	15 ± 3
Thyroid	0.21 ± 0.11	4.6 ± 0.5	0.016 ± 0.009	10 ± 6
Urinary bladder§			0.13 ± 0.03	7.5 ± 2.6
Remainder			4.0 ± 0.7	
Total body	91.0 ± 6	5.5 ± 0.2	7.5 ± 0.4	

*Uptake values are corrected for physical decay.
†Results are from fit with single exponential.
‡Computed as 2× left kidney uptake (10.5% ± 2.8%).
§Dynamic bladder model (*16*); voiding interval = 4 h; biologic half-life of activity in total body from individual measurements (average, 62 ± 13 h); fraction of activity to urine = 0.75.

fraction of the injected activity present in an organ, is also shown in Table 1.

An estimate of the fractions of activity excreted in urine and feces was calculated from the following numbers. In the first 20 h, the total fraction of activity excreted was 21.3% ± 6.3%, which was taken as $F_{urine,20h}$. During this time interval, 6.6 ± 2%ID appeared in the colon ($F_{colon,20h}$). From this, it was inferred that 24% ± 10% of the total activity that leaves the body goes to the stool, and 76% ± 10% goes to the urine.

The residence time for the bladder is estimated according to the dynamic bladder model (*16*). In this model the biologic half-life of the activity in the total body was taken as representative for the compartment feeding urine excretion. Patient-specific values were used; the average biologic half-life was 62 ± 13 h, and the range was 41–79 h. The fraction of activity excreted in the urine was taken as 0.75, as derived above.

Some organ doses are given in the last column of Table 1. These data are part of the output of the MIRDOSE 3.1 program, and they are given per injected megabecquerel of ^{99m}Tc-i-AnxV. It was seen that the kidneys received the highest dose, followed at some distance by the spleen, liver, and testes. The effective dose was found to be 9.7 ± 1.0 μSv/MBq.

Performing the analysis with the counts-to-activity conversion factor obtained from total-body activity and injected dose gave similar results for the effective dose per unit injected activity; the estimate was lower by 9% ± 8%. When organ activity was assumed to change linearly between measured points, as is implicitly done when using the trapezoidal rule for integration, the effective dose was ~7% higher than for the exponential interpolation. Not correcting for background had a more serious effect on estimated effective dose: an increase of about 36%, largely the result of an apparent increase in testes dose. Also, the estimated RM dose and the thyroid dose increased by a factor of ~2.

DISCUSSION

Scintigraphy directed at identifying an area of increased apoptosis caused an effective dose of 5.8 ± 0.6 mSv when ^{99m}Tc-i-AnxV was used in a typical dose of 600 MBq. The absorbed dose in the kidneys was 56 mGy and in the other organs was <15 mGy. The effective dose per unit of administered activity, 9.7 μSv/MBq, was in the mid range of values for the more common ^{99m}Tc compounds (*19*). From a dosimetric point of view, this makes ^{99m}Tc-i-AnxV well suited for the study of apoptosis in patients.

Uptake in the infarcted area of the heart was very limited, and no uptake was visible in the colon affected by Crohn's disease. No clear differences in activity distribution in the various patients and volunteers were observed. Because, moreover, all patients had normal kidney and liver functions, we felt justified in analyzing the data of all persons as a single representative set.

The percentage of ^{99m}Tc bound to annexin V was 82% ± 12%. Assuming that the free ^{99m}Tc is in the form of pertechnetate, the effective dose caused by pure ^{99m}Tc-i-AnxV could be estimated. Given that ^{99m}Tc-pertechnetate cause an effective dose of 13 μSv/MBq (*19*), correcting for a presence of 18% free ^{99m}Tc yields an effective dose of 9.0 μSv/MBq for 100%-labeled annexin V, compared with 9.7 μSv/MBq for the mixture. The effect on thyroid-absorbed dose would be somewhat larger—a decrease from 10 to 7.4 μGy/MBq.

The high uptake in the kidneys and the liver probably precludes the use of ^{99m}Tc-i-AnxV for the study of apoptosis in these organs or in their immediate vicinity. Also, the slow clearance from the blood is not optimal for imaging. It is interesting that the biodistribution in rats after injection of ^{99m}Tc-HYNIC-annexin V (*1*) is similar to that of ^{99m}Tc-i-AnxV in humans with respect to relative uptake in the kidneys and the liver. In both cases the kidneys show the highest uptake, followed by the liver. The absolute uptake in rats, however, was a factor of 1.5–2 higher, and blood clearance in rats was reported to occur with a half-life of <5 min (*1*). In humans, blood clearance takes place with a fast (14-min) and slow (4.1-h) component of approximately equal amplitudes. Both biodistribution and radiation dose depend on the properties of the protein as well as the prosthetic group, which is conjugated to annexin V to bind ^{99m}Tc. With other ligands, imaging properties might, in principle, still be improved.

In this study, estimation of RM-absorbed dose was based on the uptake in the iliac crests. If no background correction was applied, a doubling of the estimated RM dose of 5.5–11 μGy/MBq was seen. This illustrates that the result was rather sensitive to a correct implementation of background subtraction. The impact on the effective dose, however, would be small, because the contribution of RM was limited to ~7%. Note that activity in the RM was cleared more slowly than that in blood; the biologic half-life for RM was ~33 h, and that for the slowly cleared component in blood was 4.1 ± 1.2 h. This indicated some binding of activity in the RM. Nevertheless, it was interesting to estimate RM dose (D_{RM}) from blood and body activity neglecting this binding, because this will give a lower limit of the dose and may serve as a check. Using the method for no RM binding proposed by Shen et al. (*20*), one has the following relationship:

$$D_{RM} = \Delta_{electron} \times \phi_{electron}(RM \leftarrow RM) \times \{RMBLR \times C_{blood} - \tilde{A}_{TB}/m_{TB}\} + \hat{A}_{TB} \times S_{ref\ man}(RM \leftarrow TB) \times 69.88/m_{TB},$$

where $\Delta_{electron}$ = the total mean energy emitted per nuclear decay for electron radiation, $\phi_{electron}(RM \leftarrow RM)$ = the absorbed fraction in RM of electrons emitted in the RM itself, *RMBLR* = the RM-to-blood activity concentration ratio, C_{blood} = the cumulated radioactivity concentration in blood, $\tilde{A}_{TB}$ = the cumulated radioactivity in total body,

$S_{\text{ref man}}(RM \leftarrow TB)$ = the S value for source total-body and target RM, 69.88 = the mass of the reference man in kilograms, and m_{TB} = the mass of the patient under consideration. From our measurements we found that $C_{\text{blood}} = 9.72 \times 10^{11}$ Bq · s/kg and $\tilde{A}_{\text{TB}} = 1.51 \times 10^{13}$ Bq · s. Taking m_{TB} as the mass of reference man, $RMBLR = 0.36$ (*20*), $\phi_{\text{electron}}(RM \leftarrow RM) = 1$ for the low-energy electrons of ^{99m}Tc, $\Delta_{\text{electron}} = 2.77 \times 10^{-15}$ Gy · kg/(Bq · s) (*21*), and $S_{\text{ref man}}(RMTB) = 1.43 \times 10^{-16}$ Gy/(Bq · s) (*13*), one finds that $D_{\text{RM}} = 2.5$ mGy. This value is slightly lower than the 3 mGy found from the activity in the iliac crests. Such a result would be expected, because the method of Shen et al. neglects activity bound in the RM.

The calculation of the fractions of the injected dose that are excreted in the urine and stool was based on image data, because collection of urine and feces outside the department proved impractical. Although the images showed that probably no activity left the body by defecation, minor amounts in the feces could not be excluded because of the limited in vivo detection sensitivity. It was noted, however, that the normal intestinal transit time is about 40 h, twice the time interval considered here. For the estimated effective dose, an uncertainty in excretion route hardly has consequences; for example, varying the fraction in the urine between values as different as 50% and 100% results in a variation in effective dose of only 0.2 μSv/MBq.

In this study, corrections for attenuation and scatter were performed according to the method of depth-independent buildup factor introduced by Siegel (*14*,*15*). Implemented in software, the method is quite convenient, although it requires two parameters that must be determined experimentally. These are the buildup factor at infinite depth and a parameter that models the dependence of the attenuation coefficient on the size of the organ region of interest. Organ depth can be calculated iteratively from the ratio of counts in anterior and posterior views. Although Siegel's method is theoretically more accurate than using a counts-to-activity conversion factor obtained from total body counts and injected doses, only slightly lower results (9%) were found with the latter method.

Because the number of whole-body scans per individual is always limited, organ activity is registered at only a few points in time. The problem of interpolation of organ activity, as well as extrapolation to time zero and infinity, needs therefore to be solved before residence times can be calculated. In this study, measured points were used in pairs to construct an exponential through each pair. The first function was extrapolated to time zero and the last to infinity. Compared with using a linear function, as is effectively done during integration with the trapezoidal rule, the present method should give slightly more accurate results, because washout and decay curves generally behave exponentially rather than linearly.

CONCLUSION

The apoptosis marker ^{99m}Tc-i-AnxV strongly accumulates in the kidneys and to a lesser degree in the liver. It has a long biologic half-life of 62 ± 13 h for activity in the total body. The effective dose is 9.7 ± 1.0 μSv/MBq, corresponding to a total effective dose of 5.8 ± 0.6 mSv for a nominally injected activity of 600 MBq.

ACKNOWLEDGMENTS

The authors thank Marie Thérèse Pakbiers for help in data acquisition and analysis and Sylvia Esten for help in data acquisition.

REFERENCES

1. Blankenberg FG, Tait JF, Strauss HW. Apoptotic cell death: its implications for imaging in the next millennium. *Eur J Nucl Med*. 2000;27:359–367.
2. Fadok VA, Voelker DR, Campbell PA, Cohen JJ, Bratton DL, Henson PM. Exposure of phosphatidylserine on the surface of apoptotic lymphocytes triggers specific recognition and removal by macrophages. *J Immunol*. 1992;148:2207–2216.
3. Zwaal RF, Schroit AJ. Pathophysiologic implications of membrane phospholipid asymmetry in blood cells. *Blood*. 1997;89:1121–1132.
4. van Heerde WL, de Groot PG, Reutelingsperger CPM. The complexity of the phospholipid binding protein annexin V. *Thromb Haemost*. 1995;73:172–179.
5. van Engeland M, Nieland LJW, Ramaekers FCS, Schutte B, Reutelingsperger CPM. Annexin V-affinity assay: a review on an apoptosis detection system based on phosphatidylserine exposure. *Cytometry*. 1998;31:1–9.
6. van den Eijnde SM, Luijsterburg AJM, Boshart L, et al. In situ detection of apoptosis during embryogenesis with annexin V: from whole mount to ultrastructure. *Cytometry*. 1997;29:313–320.
7. Martin SJ, Reutelingsperger CPM, McGahon AJ, et al. Early redistribution of plasma membrane phosphatidylserine is a general feature of apoptosis regardless of the initiating stimulus: inhibition by overexpression of Bcl-2 and Abl. *J Exp Med*. 1995;182:1545–1556.
8. van den Eijnde SM, Boshart L, Reutelingsperger CPM, De Zeeuw CI, Vermey-Keers C. Phosphatidylserine plasma membrane asymmetry in vivo: a pancellular phenomenon which alters during apoptosis. *Cell Death Differentiation*. 1997;4:311–316.
9. Blankenberg FG, Katsikis PD, Tait JF, et al. In vivo detection and imaging of phosphatidylserine expression during programmed cell death. *Proc Natl Acad Sci USA*. 1998;95:6349–6355.
10. Blankenberg FG, Katsikis PD, Tait JF, et al. Imaging of apoptosis (programmed cell death) with ^{99m}Tc annexin V. *J Nucl Med*. 1999;40:184–191.
11. Hofstra L, Liem IH, Dumont EA, et al. Visualisation of cell death in vivo in patients with acute myocardial infarction, *Lancet*. 2000;356:209–212.
12. Buijs WCAM, Siegel JA, Boerman OC, Corstens FHM. Estimation of absolute organ activity using five different methods of background correction. *J Nucl Med*. 1998;39:2167–2174.
13. Stabin MG. MIRDOSE: personal computer software for internal dose assessment in nuclear medicine. *J Nucl Med*. 1996;37:538–546.
14. Siegel JA. The effect of source size on the buildup factor calculation of absolute volume. *J Nucl Med*. 1985;26:1319–1322.
15. Techniques for quantitative radiopharmaceutical biodistribution data acquisition and analysis for use in human radiation dose estimates. MIRD Pamphlet 16. *J Nucl Med*. 1999;40:37S–61S.
16. Cloutier R, Smith S, Watson E, Snyder W, Warner G. Dose to the fetus from radionuclides in the bladder. *Health Phys*. 1973;25:147–161.
17. Buijs WCAM, Oyen WJG, Dams EThM, et al. Dynamic distribution and dosimetric evaluation of human nonspecific immunoglobulin G labeled with In-111 or Tc-99m. *Nucl Med Commun*. 1998;19:743–751.
18. International Commission on Radiological Protection. *Basic Anatomical and Physiological Data for Use in Radiological Protection: the Skeleton*. ICRP Publication 70. Oxford, UK: Pergamon Press; 1995.
19. International Commission on Radiological Protection. *Radiation Dose to Patients from Radiopharmaceuticals. Addendum to ICPR Publication 53*. Oxford, UK: Pergamon Press; 1998.
20. Shen S, DeNardo GL, Sgouros G, O'Donnel RT, DeNardo SJ. Practical determination of patient specific marrow dose using radioactivity concentration in blood and body. *J Nucl Med*. 1999;40:2102–2106.
21. Loevinger R, Budinger TF, Watson EE. *MIRD Primer for Absorbed Dose Calculations*. New York, NY: The Society of Nuclear Medicine; 1988.